Electronic structure of graphene nanoribbons on hexagonal boron nitride

Yohanes S. Gani, D. S. L. Abergel, and Enrico Rossi

Phys. Rev. B **98**, 205415 — Published 21 November 2018

DOI: 10.1103/PhysRevB.98.205415

Electronic structure of graphene-nanoribbons on hexagonal boron nitride.

Yohanes S. Gani[1], D.S.L. Abergel[2*], Enrico Rossi[1]
[1]*Department of Physics, William & Mary, Williamsburg, VA 23187, USA*
[2]*Nordita, KTH Royal Institute of Technology and Stockholm University, Roslagstullsbacken 23, 10691 Stockholm, Sweden*
(Dated: October 24, 2018)

Hexagonal boron nitride is an ideal dielectric to form two-dimensional heterostructures due to the fact that it can be exfoliated to be just few atoms thick and its a very low density of defects. By placing graphene nanoribbons on high quality hexagonal boron nitride it is possible to create ideal quasi one dimensional (1D) systems with very high mobility. The availability of high quality one-dimensional electronic systems is of great interest also given that when in proximity to a superconductor they can be effectively engineered to realize Majorana bound states. In this work we study how a boron nitride substrate affects the electronic properties of graphene nanoribbons. We consider both armchair and zigzag nanoribbons. Our results show that for some stacking configurations the boron nitride can significantly affect the electronic structure of the ribbons. In particular, for zigzag nanoribbons, due to the lock between spin and sublattice degree of freedom at the edges, the hexagonal boron nitride can induce a very strong spin-splitting of the spin polarized, edge states. We find that such spin-splitting can be as high as 40 meV.

PACS numbers: 73.22.Pr, 72.80.Vp, 73.63.Nm, 85.35.-p

I. INTRODUCTION

Graphene nanoribbons (GNRs)[1–8] are almost ideal 1D electronic systems: they are only one atom thick and their width can be just few atoms. Recent advances in bottom-up synthesis using molecular precursors allow to control with atomic precision the width and the edges' morphology of GNRs.[9–12]. These developments make GNRs very promising as basal elements for the realization of quasi-1D systems and 1D topological states[13,14]. The particular advantage of GNRs toward this goal are: (i) almost ideal 1D character, (ii) scalable synthesis and layout to create networks of quasi 1D channels, (iii) tunability of their electronic properties via edge and width engineering. Interest in 1D electronic systems has recently increased substantially given that to date the most successful and promising approaches to realize non-abelian electronic states, such as Majoranas, rely on the availability of 1D devices[15] of high quality (ideally disorder free)[16–24]. The ultimate 1D nature of GNRs and therefore large energy separation between their 1D subbands makes them in many respects ideal for the realization of 1D superconductor heterostructures compared semiconductor-superconductor nanowires where in typical experimental conditions several bands are occupied[25–27].

To be able to use GNRs to realize states like Majoranas[28] the GNRs have to be of very high quality, i.e to have a very low level of disorder. In recent years high quality hexagonal boron nitride, hBN, has emerged as the ideal dielectric to realize graphene-based heterostructures[29–33]. This is due to the fact that hBN has a large band gap, a very low density of impurities and crystal defects, and it can be exfoliated to be only few atoms thick. Because of the extreme low impurity density of hBN, graphene devices in which hBN is the dielectric substrate have electron's mobilities orders of magnitude larger than graphene devices on other substrate, such as, for example, silicon dioxide[34–39]. One additional important consequence of having a substrate with low disorder, is that in systems like graphene and bilayer graphene, it also reduces the carrier density inhomogeneities that, especially close to the Dirac point or in the presence of a small band gap, can be very large and significantly modify the electronic properties of the graphene-based device[40–55]. Imaging experiments have directly shown that the use of hBN as a substrate instead of silicon oxide greatly reduces the amplitude of the disorder-induced carrier density inhomogeneities[31,33,56].

For all the reasons stated above it is natural to use hBN as a substrate for graphene nanoribbons. However, it has been shown both theoretically[57–61] and experimentally[33,62–65] that hBN can qualitatively affect the band structure of graphene. This is due to the fact that in graphene-hBN devices, because hBN has a lattice constant that is only 1.8% larger than graphene's, there can be region tens of nanometer wide in which the graphene layer is in register with the hBN lattice[66] and therefore have its sublattice symmetry broken given that in hBN the A and B sublattices create different electrostatic potentials. Given that GNRs are typically only few atoms wide we should expect that hBN can qualitatively modify their band structure. In order to be able to use hBN to increase the quality of GNRs to realize almost ideal 1D electronic systems, it is therefore necessary to understand how hBN can affect the spectrum of GNRs.

In this work we study how hBN modifies the band structure of GNRs. We study different types of GNRs and consider different (commensurate) stackings between the GNRs and hBN. We find that hBN can cause qualitative changes to the band structure of GNRs and that these changes can be tuned by selecting the stacking configuration. The effects are most dramatic for zig-zag graphene nanoribbons (GNRs): for such ribbons hBN in general induces a spin splitting of the conduction band (CB) and valence band (VB). We also find that the sign of such spin-splitting can be changed simply by changing, via a rigid shift, the stacking between the ZGNR and hBN.

*Present address: Nature Physics, 4 Crinan Street, London, N1 9XW, UK

The paper is organized as follows: in Sec. II we present the theoretical method that we use and a brief review of the electronic structure for isolated GNRs and hBN, in Sec. III we present the results for the band structure of GNR-hBN heterostructures, and in Sec. IV we provide our conclusions.

II. METHOD

Graphene is a one-atom thick layer of carbon atoms arranged in an hexagonal structure[34,39,67,68]. In graphene the carbon-carbon distance, a, is 1.46 Å. The hexagonal structure is best described as a triangular lattice with lattice constant $a_G = \sqrt{3}a$ and a basis with two sites, A and B. The atoms at sites A form the A-sublattice and the atoms at the B sites form the B-sublattice. In graphene the A and B sites are both occupied by carbon atoms and so we have sublattice symmetry. Graphene nanoribbons can be obtained by etching graphene along particular directions[69]. More recently, GNRs have been produced via bottom-up synthesis[9–11], a fabrication technique that allows to control with atomic precision the width of the ribbon and the shape of their edge and therefore their electronic properties. Depending on their edges we can identify two types of GNRs: armchair GNRs (AGNRs), Fig. 1 (a), in which the edges look like a sequence of armchairs, and zigzag GNRs (ZGNRs), Fig. 1 (b), in which the edges have a zigzag pattern. It is customary to refer to the width of an AGNR via the number N across the transverse direction of carbon-carbon dimers aligned along the longitudinal direction. For ZGNRs the width is denoted by the number N of zigzag chains. For the remainder it is important to notice that the unit cell of AGNRs and ZGNRs is different, as shown in Fig. 1. Let $a_{\rm AGNR}$ be the nanoribbon lattice constant. For AGNRs $a_{\rm AGNR} = \sqrt{3}a_G$, for ZGNRs $a_{\rm ZGNR} = a_G$.

The heterostructures that we study are formed by a graphene nanoribbon (armchair of zigzag) placed on hBN. Figure 1 (c-f) show some examples GNR-hBN structures. In hBN the sublattice A (B) is occupied by boron (nitrogen) atoms, or vice versa. The fact that the A and B sites are not equivalent in hBN in Fig. 1, and all the figures in the remainder of this work, is denoted by the fact that they are shown in different colors. In all the results presented in the remainder, to avoid the effects due to dangling bonds, we assume the edges of the GNRs to be terminated by hydrogen atoms, showing in light grey in Fig. 1. It is helpful to name the particular stackings shown in Fig. 1. Figure 1 (c) shows the case in which the ribbon and the hBN are in the AA stacking configuration, i.e. the case in which the GNR's sublattice A (B) is directly above the sublattice A (B) of hBN. In the AB_N (AB_B) stacking the sublattice A (B) of the GNR is in register with the sublattice occupied by the nitrogen (boron) atoms of the substrate, Fig. 1 (d) (Fig. 1 (e)). In the bridge-stacking configuration, $\rm A_{br}$, the carbon-carbon links of the GNR cross the boron-nitrogen links of the substrate, Fig. 1 (f).

The tight-binding model is a computationally very efficient method that has been used to obtain the band structure of GNRs[1,70–72] and related systems. However, to get accurate results, even qualitatively, using the tight-binding model requires a fine tuning of its parameters that can only be achieved by comparing the tight-binding model's results to the ones obtained using density functional theory (DFT) approaches[3,5,6,73–75]. For the case of isolated AGNR this is exemplified by the fact that the simple nearest neighbor tight binding model with constant hopping parameter for the case in which $N = 3n-1$ return a gapless band-structure whereas DFT shows the presence of finite band-gap[5,6]. The main reason for such discrepancy is that, due to the finite width of the ribbon, the hopping parameter entering the tight-binding model should not be taken to be constant across the ribbon's

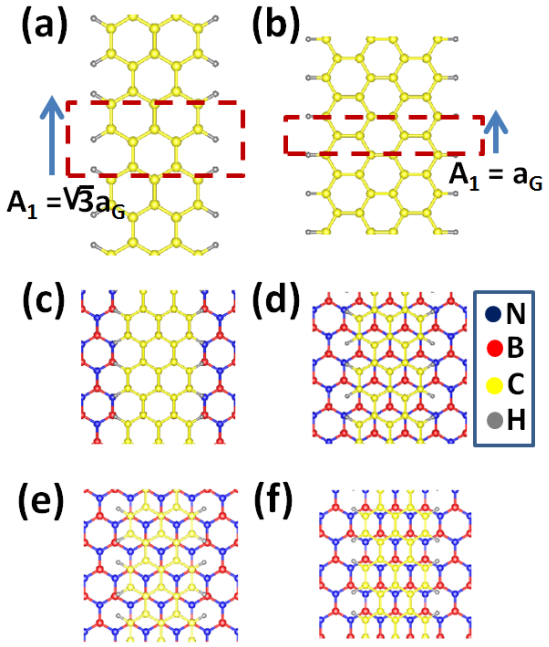

FIG. 1: Atoms layout for AGNR (a), and ZGNR (b). The dashed lines identify the primitive cells. (c), (d), (e), (f) possible stacking configurations between a GNR and hBN: AA, $\rm AB_N$, $\rm AB_B$, and $\rm A_{br}$, respectively.

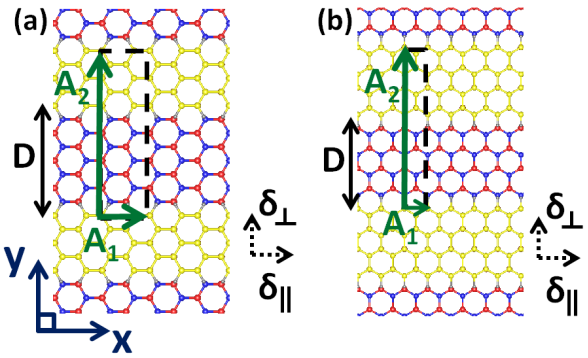

FIG. 2: Sketch of the supercell used for the DFT calculation. D is the distance between ribbons, and $\delta_\perp$ ($\delta_\parallel$) denote transverse (longitudinal) shifts of the GNR with respect to the hBN substrate away from AA stacking.

width[5] and hopping processes beyond next-neighbor should also be included[70]. For ZGNRs the simple tight-binding model predicts a gapless band structure, due to the presence of edge modes, a fact that is not affected by the variation of the hopping parameter across the ribbon. However, also for ZGNRs the result of the simple tight-binding model are qualitatively incorrect if one does not include the effect of the exchange part of the Coulomb interaction. The exchange interaction causes ZGNRs to have an insulating ground state with ferromagnetic order along the edges and antiferromagnetic order between the two edges, effect that is correctly captured by ab-initio calculations[76–78]. As evidence of the significant advances in the syntesis of high quality GNRs, very recently the ZGNRs' magnetic edges states have been observed experimentally[12]

For the reasons stated above, in this work we obtain the electronic structure of all the systems via ab-initio density functional theory calculations using the Quantum Espresso package[79]. We use ultrasoft potentials and a plane-waves basis with periodic boundary conditions.

We denote as x the axis along the longitudinal direction of the GNR, as z the axis perpendicular to the heterostructure plane and as y the axis in the GNR plane perpendicular to both x and z, as shown in Fig. 2. $\delta_{\parallel}$ ($\delta_{\perp}$) denotes a shift along the x (y) direction between the GNR and the substrate. In order to simulate a heterostructure with an isolated GNR we need to use a supercell large enough to minimize artificial interference effects arising from the periodic boundary conditions. We find that for supercell sizes $D > 9a_G$ finite size effects are negligible and do not affect the electronic structure of the GNR. In the direction perpendicular to the plane of the GNR-hBN heterostructure we insert a "vacuum layer" 10 Å thick.

The electron exhange and correlation are calculated by implementing the generalized gradient approximation (GGA) functional of Perdew-Burke-Ernzerhof (PBE)[80]. For AGNR hybrid systems the Brillouin zone (BZ) integration is performed by generating a uniform 12x12x1 mesh of k points using the Monkhorst-Pack procedure. For ZGNR hybrid systems we use the same procedure using 16x16x1 mesh. The cut off energy wavefunction and charge densities are set to be 50 Ry and 400 Ry, respectively, ensuring the convergence of the total energy. To be able to compare the effect of different stacking configurations we keep the interlayer distance d fixed. We conservatively set $d = 3.5$Å considering that the modifications of the GNR electronic structure due to the presence of the substrate are stronger for smaller values of d. Changes in d do not change qualitatively the results that we present in remainder.

We limit ourselves to the case when the stacking between the nanoribbon and hBN is commensurate . We assume that the 1.8% lattice mismatch between the graphene nanoribbon and hBN can be neglected given the small size of the system and the fact that in graphene-hBN heterostructures it has been shown that graphene and hBN lattices can be in commensurate stacking configurations over regions tens of nanometers wide. wide[66].

III. RESULTS

In this section we present our results. To better understand the results for the GNR-hBN heterostructures it is helpful to briefly review the electronic structure of isolated GNRs and hBN. Figure 3 shows the low-energy band structure of isolated GNRs obtained using DFT, see Sec. II. Figures 3 (a)-(c) show the band structure for AGNRs with width $N = 3n - 1$, $N = 3n$, $N = 3n + 1$, respectively for the case when $n = 2$. As discussed in Sec. II for all three cases we have a gapped band structure. Figure 3 (d) shows the band structure for a ZGNR of width $N = 4$. Notice that for a ZGNR the low energy states are located at the edge of the 1D BZ ($k = \pi/a_{\mathrm{ZGNR}}$), and the gap due to the antiferromagnetic ordering, decreases with the width of the ribbon. Here, and in the remainder, $\Delta^{(0)}$ denotes the direct band gap and $\Delta^{(1)}$ the energy splitting for $k = \pi/a_{\mathrm{ZGNR}}$. Figure 4 shows the low energy band structure of hBN.

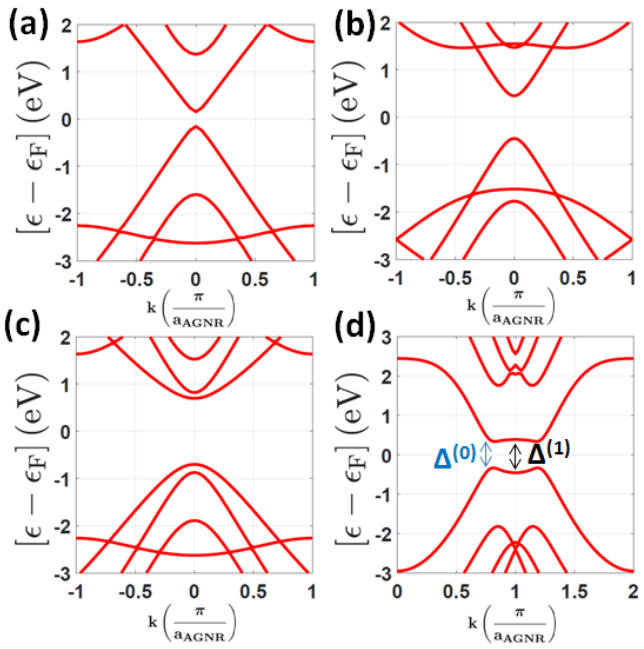

FIG. 3: (a) Band structure for an AGNR with N=3n-1=5, (n=2). (b) Band structure for an AGNR with N=3n=6. (c) Band structure for an AGNR with N=3n+1=7. (d) Band structure for a a ZGNR with N=4.

A. AGNR-hBN heterostructures

In this section we present the results for heterostructures formed by AGNR and hBN. Figure 5 (a) shows the low-energy band-structure of a AGNR-hBN heterostructure in the AA stacking configuration: here and in the remainder the dashed lines show the spectrum of the isolated GNR and the solid lines the spectrum of the heterostructure. We see that for this configuration the presence of the hBN does not modify significantly the spectrum of the GNR. Figure 5 (b) shows the shift

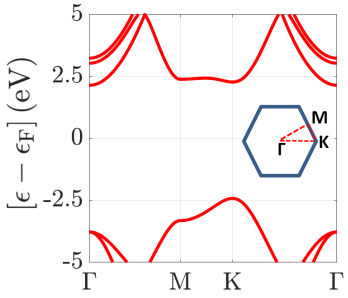

FIG. 4: Low energy band structure of hBN. The inset shows the Brillouin Zone.

in energy of the ribbon valence and conductance band due to the presence of the hBN: we see that for this configuration the variation in energy is of the order of 15 meV close to the $k = 0$ point and slowly increases (in absolute value) as we move away from $k = 0$.

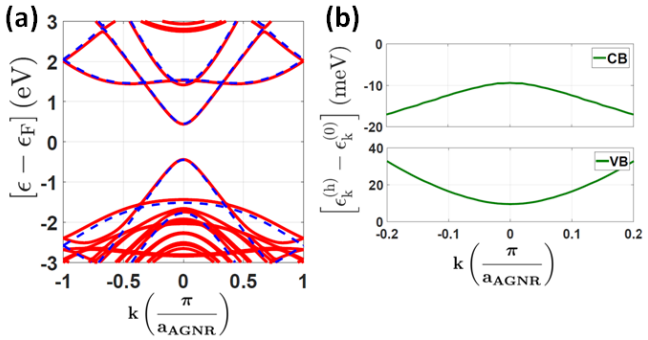

FIG. 5: (a) Bands of a AGNR-hBN heterostructure for a ribbon with $N = 6$ placed on hBN in the AA stacking configuration. The dashed lines show the spectrum of the isolated GNR and the solid lines the spectrum of the heterostructure. (c), (d) energy shift as a function of k of the CB, and VB, respectively.

To study how differences in stacking affect the spectrum we studied the effect of a shift away from the AA configuration in the longitudinal and transverse direction. The relative change of the ribbon's band gap $\Delta_r \equiv (\Delta_h - \Delta_0)/\Delta_0$ where Δ_h is the band gap of the GNR-hBN heterostructure, can be used to show in a compact way the effect. The results are shown in Fig 6 for the three classes of AGNRs: $N = 3n - 1$, $N = 3n$, $N = 3n + 1$ where, as in the remainder of this work, we have taken $n = 2$. We see that a shift in the perpendicular direction has only a minor effect: the relative change is at most of the order of 2%. We also observe that the highest increase of the band gap due to $\delta_\perp$ is obtained when the shift results in the A_{br} configuration for $N = 3n - 1$ and $N = 3n + 1$ AGNRs and very close to it for $N = 3n$ AGNRs.

The shift in the longitudinal direction has a stronger effect than $\delta_\perp$. By varying $\delta_\parallel$ we can obtain the AB_N and AB_B configurations. Figure 6 shows that for all the three types of ribbons $\Delta_r(\delta_\parallel)$ has an extremum when the AB_B configuration is realized. For most cases a shift in the longitudinal direction can induce a change of the band gap of the order of 6% or less, however, for the case when $N = 3n - 1$, i.e. for the class of AGNRs for which Δ_0 is the smallest (zero using a tight binding model with uniform hopping parameters) a shift in the longitudinal direction away from the AA stacking can lead to a configuration for which the band gap is reduced by 20%, i.e. about 60 meV in absolute terms. Figure 7 shows the atoms arrangement for this configuration, and the corresponding low-energy band-structure. We see that for this stacking the nitrogen atoms are located midway under the longitudinal C-C bonds.

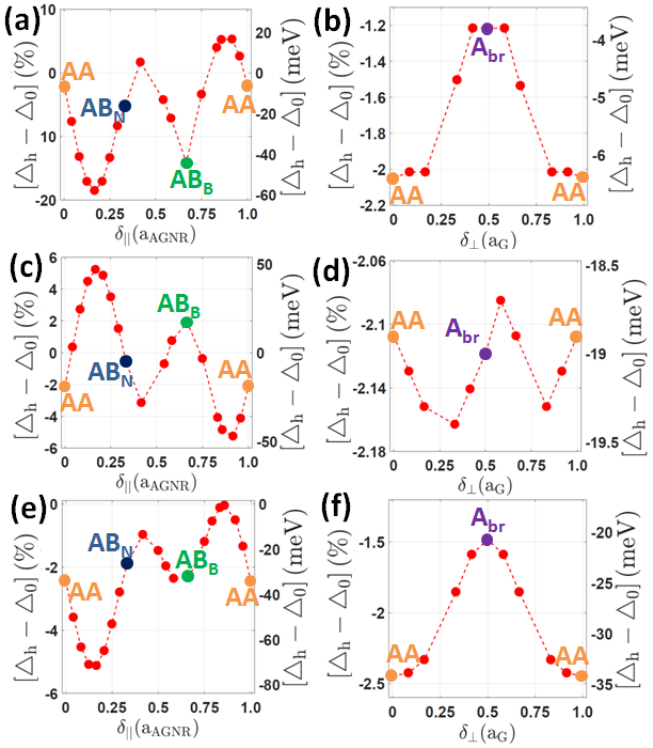

FIG. 6: Evolution of the band gap of a AGNR (with $n = 2$) placed on hBN as a function of shift away from AA stacking. The left panels show the results for a shift along $\delta_\parallel$, the right panels for shifts along $\delta_\perp$. The different rows show the results for different widths of the ribbon: the first row (panels (a) and (b)) show the results for the case when $N = 3n - 1 = 5$, the second (panels (c) and (d)) for the case when $N = 3n = 6$, and the last (panels (e) and (f)) for the case when $N = 3n + 1 = 7$.

We expect that graphene nanoribbons will be placed on hBN via methods (such as exfoliation) that in general lead to long-lived metastable stacking configurations that are not the thermodynamic ground state. However, it can be insightful to see which configurations, among the ones considered in Fig. 6, are the most stable. For this reason we calculated the change, with respect to the AA-stacking configuration, of the total energy as a function of $\delta_\parallel$ and $\delta_\perp$. Figure 8 show the results for the case of an AGNR with $N = 6$ (we find the same qualitative results for different values of N). This figure shows that the AB_B stacking configuration is the most stable,

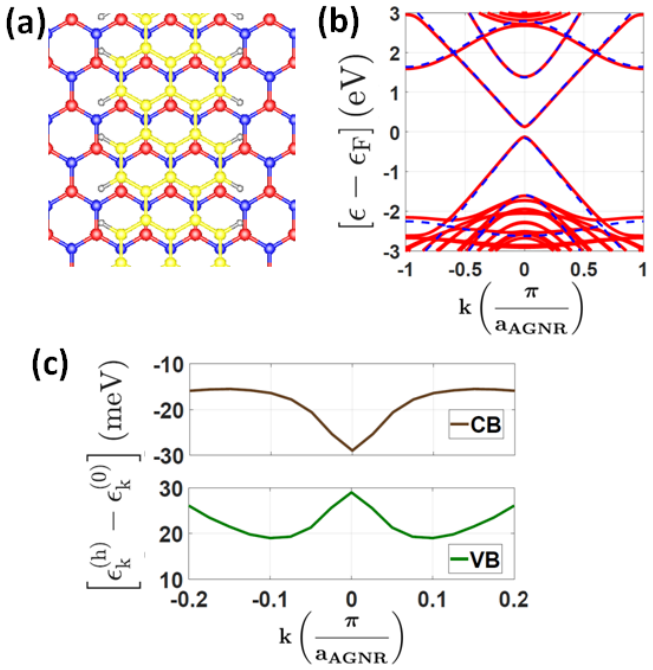

FIG. 7: (a) Stacking configuration for a AGNR-hBN system corresponding to the maximum gap change shown in Fig. 6 (a) ($N = 5$) corresponding to $\delta_{||} = 0.16\left(\frac{1}{a}\right)$. (b) Bands for the stacking configuration shown in (a) (the dashed lines show the bands for the isolated ribbon). (c) The top panel shows the difference at small k's between the heterostructure's conduction band, CB, and the isolated ribbon's CB for the stacking configuration shown in (a). The bottom panel show the difference between the VBs.

in agreement with previous studies of graphene on hBN[60].

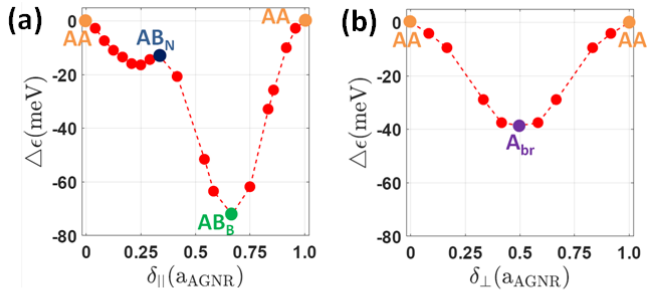

FIG. 8: (Color online) Change of the total energy, with respect to the case of AA stacking, as a function of $\delta_{||}$ (a), and $\delta_{\perp}$ (b), for an AGNR with $N = 6$ placed on hBN

B. ZGNR-hBN heterostructures

We now consider ZGNR-hBN heterostructures. Figure 9 shows the low energy spectrum of a ZGNR-hBN heterostructure for the case of AA stacking. Analogously to what we find for AGNR-hBN we see that for this configuration the effect of the hBN on the band gap is small: the conduction and valence bands around $k = \frac{\pi}{a_{ZGNR}}$ are shifted by 10-20 meV, Fig. 9 (c). However, the presence of hBN causes an important qualitative modification of the band structure: it induces a spin splitting of the valence and conduction bands, see Fig. 9 (d). This is due to the locking between spin and sublattice degrees of freedom for the edge states[81] and the fact that the presence of hBN breaks the GNR sublattice symmetry. For ZGNRs the left (right) edge state has spin polarization up (down) while at the same time the atoms forming the left (right) edge belong to the A (B) sublattice (or viceversa). As Fig. 10 shows the presence of hBN breaks the sublattice symmetry and therefore the degeneracy of the states due to this symmetry. In a ZGNR, the breaking of the sublattice symmetry therefore causes a spin splitting of the edge states, for which spin and sublattice degrees of freedom are locked. Such spin splitting is not affected qualitatively by changes in the interlayer distance d, however, changes in d have quantitative effects: as we would expect decrease of d increases the spin splitting as confirmed by the comparison of the results shown in Fig. 10 (e) and Fig. 10 (f) that were obtained using $d = 3.5$Å and $d = 3.4$Å, respectively.

The effect of the presence of hBN on the band structure of ZGNR is similar to the effect of an electric field applied along the transverse direction of a ZGNR. It was shown that for large enough transverse electric fields a ZGNR can be driven into an ideal half-metallic state[82,83]. For the case of a ZGNR placed on hBN the difference in electrostatic potential between the ZGNR's atoms on the two different edges is not due to an external electric field but the fact that they are located above different atoms of the layer forming the substrate. The results of Figure 9 (d) show that hBN, and any substrate that break the sublattice symmetry of graphene, can be used to spin split the edge modes of a ZGNR. We can conclude that in ZGNR-hBN heterostructures we can break the spin-degeneracy without having to introduce an external magnetic field and explicitly breaking the time reversal symmetry. It is interesting to see if such an effect can be maximized by tuning the stacking configuration and the width of the ZGNR.

Figure 11 shows the effects on the ZGNR band structure of a shift along the ribbon's transverse direction away from the AA stacking configuration. We see that the reduction of $\Delta^{(0)}$ and $\Delta^{(1)}$ oscillates with $\delta_{\perp}$, Fig. 11 (a), (b). The spin splitting also oscillates with $\delta_{\perp}$ Fig. 11 (c), (d), in a very similar way both around $\Delta^{(0)}$ and $\Delta^{(1)}$ for valence and conduction band. As for the band-gap the effect of the hBN on the spin splitting is minimal for the AB_B stacking configuration. Also for values of $\delta_{\perp}$ such that a configuration between AA and AB_N is realized the spin splitting can be tuned very close to zero. We find that by varying $\delta_{\perp}$ the Zeeman splitting is maximized when a configuration close to the AB_N stacking ($\delta_{\perp} = 0.8a_G$) or not too far from the AA stacking one ($\delta_{\perp} = 1.5a_G$). For these configurations the spin splitting is about 40 meV. Fig. 11 (e), (f) show the stacking configurations corresponding to $\delta_{\perp} = 0.8a_G$ and $\delta_{\perp} = 1.5a_G$, respectively. We see that in both cases the carbon atoms of one of the GNR sublattices are very close to the nitrogen atoms

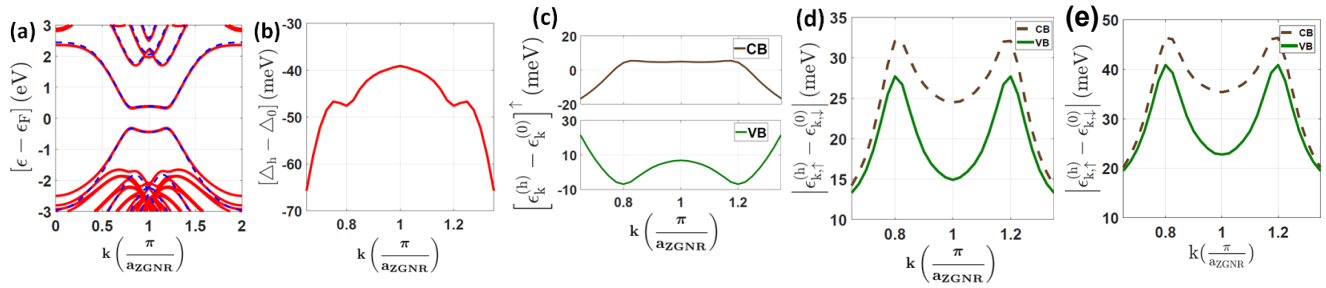

FIG. 9: Results for a ZGNR with $(N = 4)$ placed on hBN in the AA stacking configuration. (a) Band structure, the dashed lines show the bands for the isolated ZGNR. (b) Difference, for k close to $\pi/a_{\rm ZGNR}$, between the band gap of the hBN-ZGNR heterostructure, Δ_h, and the band gap of the isolated ZGNR Δ_0. (c) The top panel shows the difference for k close to $\pi/a_{\rm ZGNR}$ between the ZGNR-hBN heterostructure's CB and the isolated ribbon's CB for the AA stacking configuration. The bottom panel show the difference between the VBs. (d) Spin splitting as a function of k for the ZGNR-hBN heterostructure's CB and VB. (e) Same as (d) but for $d = 3.4$Å.

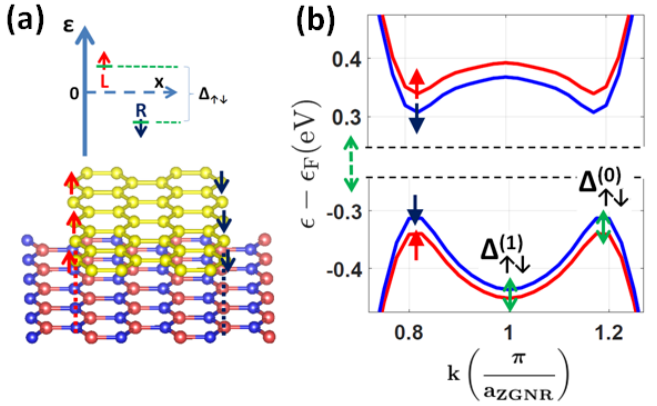

FIG. 10: (a) Sketch of a ZGNR placed on hBN in the AA stacking configuration. The arrows at the edges of the ZGNR show the spin polarization of the edge modes. (b) Enlargement of the VB and CB to show the spin splitting due to the presence of hBN.

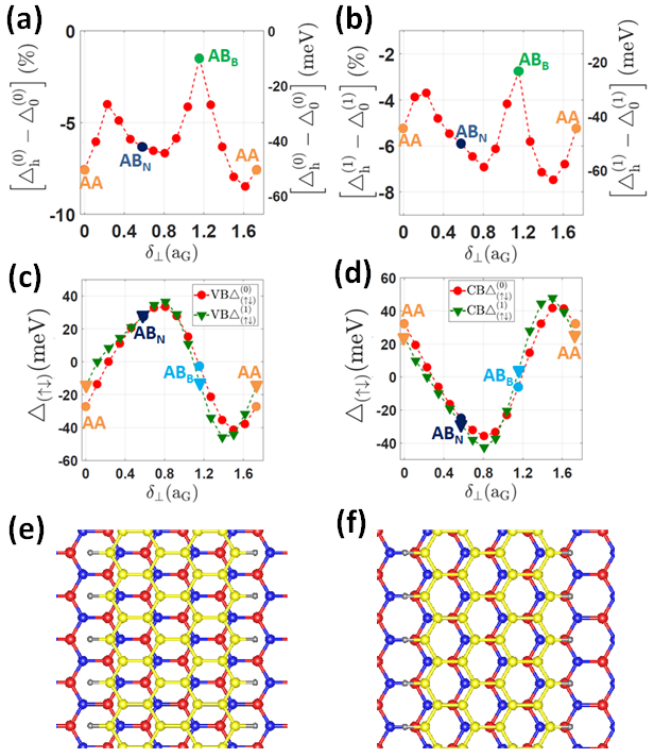

FIG. 11: Evolution of the band gaps and spin splittings of a ZGNR with $N = 4$ placed on hBN as a function of $\delta_\perp$. (a), (b), Change of $\Delta^{(0)}$, $\Delta^{(1)}$, respectively, due to the presence of the hBN. (c), (d) Spin splitting $\Delta_{(\uparrow\downarrow)}$, at $k = \pi/a_{\rm ZGNR}$, and close to $\Delta^{(0)}$, due to the presence of hBN for the VB and CB, respectively. (e), (f) Stacking configuration corresponding to the values of $\delta_\perp$ for which the spin splitting $\Delta_{(\uparrow\downarrow)}$ is maximized, shown in (c), (d): $\delta_\perp = 0.8a_G$ in (e), and $\delta_\perp = 1.5a_G$ in (f).

whereas the carbon atoms of the other sublattice are very close to the boron atoms. Due to the details of the electrostatic environment created by the hBN we conclude that these, among the configurations that we have considered, are the ones that maximize the breaking of the ZGNR sublattice symmetry and therefore the spin splitting of the spin polarized edge modes.

Figure 12 shows how the band gap and the spin splitting change by shifting the ZGNR away from the AA stacking along the longitudinal direction. As for the case of a perpendicular shift, we see that both the gap and the spin-splitting oscillate with $\delta_\parallel$. Both the gaps, $\Delta^{(0)}$ and $\Delta^{(1)}$, and the spin splitting are symmetric with respect to $(\delta_\parallel - (1/2)a_{\rm ZGNR})$ This can be understood considering that for $\delta_\parallel = (1/2)a_{\rm ZGNR}$ we obtain the $A_{\rm br}$ configuration and that shifts along the longitudinal direction around such configuration lead to equivalent stackings. The results of 12 (b)-(d) show that for the $A_{\rm br}$ configuration, see Fig. 1 (f), both $\Delta^{(1)}$ and the spin splitting are maximized. Our results show that, due to the details of the electrostatic potential created by the atoms forming the heterostructure, the strongest sublattice-breaking effect of hBN is not obtained for the AA stacking configuration, as one would naively expect, but for configurations as the ones shown in Fig. 1 (f) and Fig. 11 (e), (f) in which the carbon atoms are

slightly off from being directly above the nitrogen and carbon atoms.

Figure 14 shows the low-energy band structure of ZGNR-hBN for the A_{br} configuration. As to be expected we see, Figure 14 (c), that the spin splitting induced by the presence of hBN decreases as we move away from the $k = \pi/a_{ZGNR}$ point, i.e as we move away from the value of k for which the locking of the spin and sublattice degree of freedoms for the edge states is the strongest.

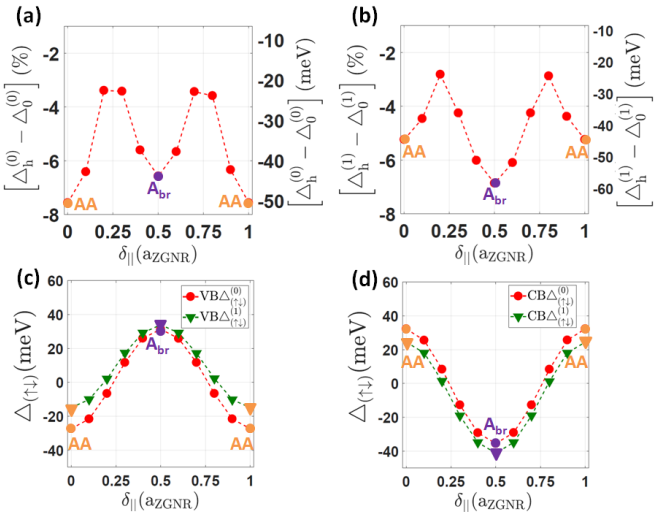

FIG. 12: Evolution of the band gaps and spin splittings of a ZGNR with $N = 4$ placed on hBN as a function of a shift $\delta_{||}$ away from AA stacking. (a) Change of $\Delta^{(0)}$ due to the presence of the hBN. (b) Change of $\Delta^{(1)}$ due to the presence of the hBN. (c), (d) Spin splitting $\Delta_{(\uparrow\downarrow)}$, at $k = \pi/a_{ZGNR}$, and close to $\Delta^{(0)}$, due to the presence of hBN for the CB and VB respectively.

We have shown for the case of AGNRs that the more stable configuration is the AB_B one, Fig. 8. We expect this to be the case also for ZGNRs. This is confirmed by the results shown in Fig. 13 in which the the change, with respect to the AA-stacking configuration, of the total energy of a ZGNR-hBN system (with $N = 4$) as a function of $\delta_{||}$ and $\delta_{\perp}$ is shown.

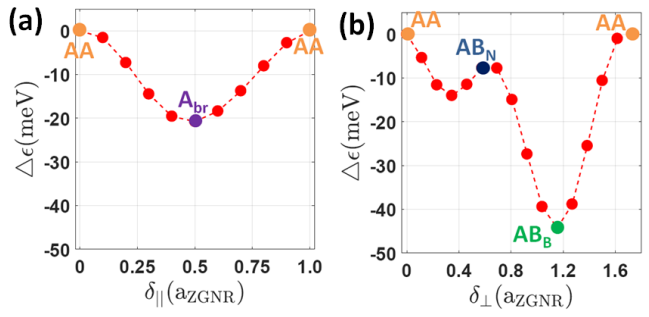

FIG. 13: (Color online) Change of the total energy, with respect to the case of AA stacking, as a function of $\delta_{||}$ (a), and $\delta_{\perp}$ (b), for an ZGNR with $N = 4$ placed on hBN

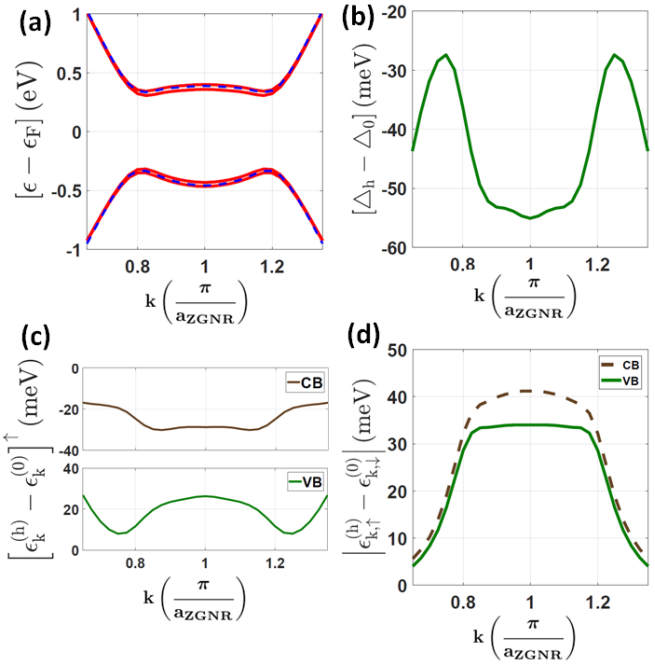

FIG. 14: Results for a ZGNR with $(N = 4)$ placed on hBN in the A_{br} stacking configuration. (a) Band structure, the dashed lines show the bands for the isolated ZGNR. (b) Difference, for k close to π/a_{ZGNR}, between the band gap of the hBN-ZGNR heterostructure, Δ_h, and the band gap of the isolated ZGNR Δ_0. (c) The top panel shows the difference for k close to π/a_{ZGNR} between the ZGNR-hBN heterostructure's CB and the isolated ribbon's CB for the AA stacking configuration. The bottom panel show the difference between the VBs. (d) Spin splitting as a function of k for the ZGNR-hBN heterostructure's CB and VB.

The results of Figs. 11, 12 show that by shifting the ZGNR away from the AA configuration we have the maximum spin splitting for shift in the transverse direction with $\delta_{\perp} = 1.5a_G$. It is then interesting to see how the main features of the band structure of a ZGNR-hBN system with $\delta_{\perp} = 1.5a_G$ vary as we change the width of the nanoribbon. The results are shown in Fig. 15. For an isolated ZGNR we have that as N increases the band gap $\Delta^{(0)}$ induced by the antiferromagnetic ordering of the edge states decreases, whereas $\Delta^{(1)}$ remains approximately constant[77]. This is shown by the squares symbols in Fig. 15 (a), and (b), respectively. The circles in the same figures show the results for the ZGNR-hBN heterostructure. We see that the presence of hBN does not affect qualitatively the scaling of of $\Delta^{(0)}$ and $\Delta^{(1)}$ with respect to N.

It is then interesting to see how the spin splitting induced by the presence of hBN scales with N. Fig. 15 (c), (d) show the spin splitting around $\Delta^{(0)}$ and $\Delta^{(1)}$, respectively. Contrary to $\Delta^{(0)}$ the spin splitting around it depends very weakly on N. This can be qualitatively understood considering that the states close to $\Delta^{(0)}$ are not strongly localized at the edges as shown in Fig. 16 (c), (d) and their localization does not change much by varying the width of the ribbon. As a consequence, the fact that the carbon atoms at the opposite edges of the ribbons see a different electrostatic potential being either on top of nitrogen atoms or boron atoms, does not cause a

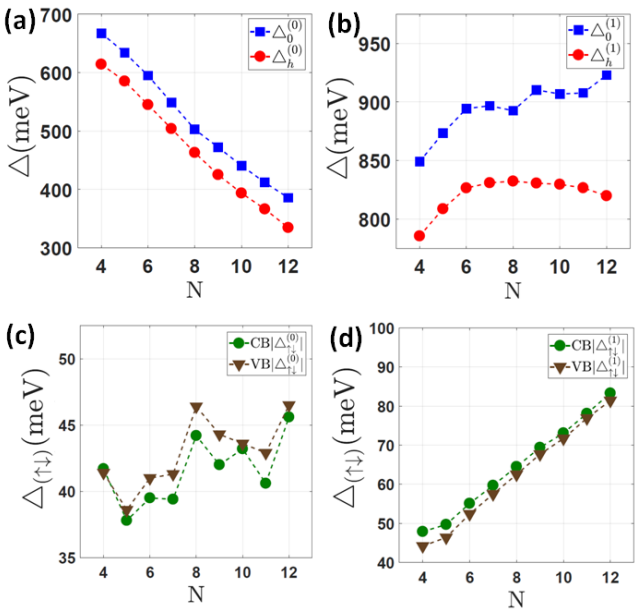

FIG. 15: Effect of the ribbon width, N for a ZGNR-hBN heterostructure with stacking configuration shown in Fig. 11 (f) corresponding to $\delta_\perp = 1.5a_G$, value of $\delta_\perp$ for which the spin splitting $\Delta_{(\uparrow\downarrow)}$ is maximized. $\Delta^{(0)}$, (a), and $\Delta^{(1)}$, (b), as a function of N for the ZGNR-hBN heterostructure and the isolated ribbon. $\Delta_{(\uparrow\downarrow)}$ for CB and VB around the X point, (c), and the $k = \pi/a_{\rm ZGNR}$, (d).

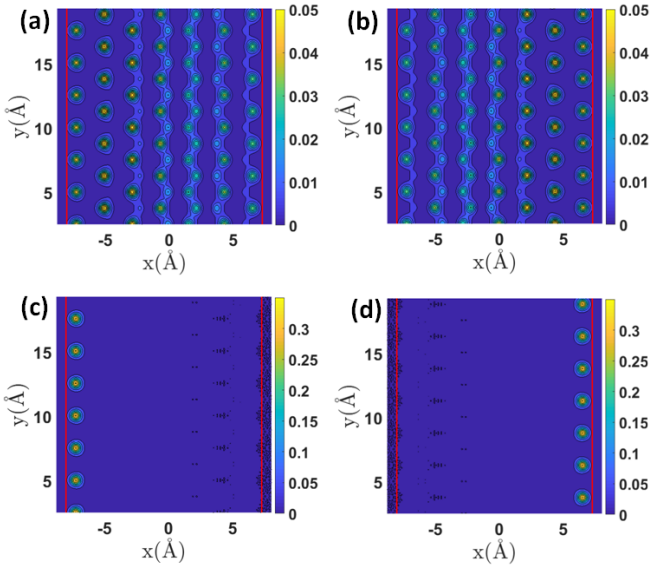

FIG. 16: Electron charge density for a pristine ZGNR with $N = 7$. (a), (b) ((c), (d)) show the electron density of spin up and spin down states, respectively close to $\Delta^{(0)}$ ($k = \pi/a_{\rm ZGNR}$).

spin splitting that depends strongly on the ZGNR's width, as shown in Fig. 15 (c). The opposite is true for the states close to $k = \pi/a_{\rm ZGNR}$: in this case the states are strongly localized to the edges and this localization increases with the ribbon's width enhancing the spin splitting due to the sublattice breaking effect of hBN on the ribbon, Fig. 15 (d). We therefore conclude that the semimetal character of ZGNRs placed on hBN can be increased by considering wider ribbons.

IV. CONCLUSIONS

We have studied how the presence of hBN affects the electronic structure of armchair and zigzag graphene nanoribbons. We have obtained how hBN modifies the low energy properties of the graphene ribbons' bands and how these changes depend on the stacking configuration. Pristine armchair graphene nanoribbons have always a finite band gap. We find that for the class of armchair graphene nanoribbons with the smallest band gap, ribbons of width $N = 3n-1$ (with n a positive integer), the presence of hBN can modify the GNR's gap by as much as 20%. For the armchair graphene nanoribbons for which the band-width is larger when isolated, ribbons of width $N = 3n$ and $N = 3n+1$, the presence of hBN modifies the size of the gap only up to about 6%.

The effect of hBN is much more significant for zigzag graphene nanoribbons. For these ribbons the band gap is due to the antiferromagnetic ordering of the edge states and the fact that the carbon atoms at the opposite edges of the ribbon belong to different sublattices implies that the presence of hBN, by breaking the sublattice symmetry, can strongly modify the low-energy features of the ribbon. The presence of hBN can induce a significant spin splitting of the conduction and valence band and drive the ribbon into a half-metallic state. We find that such spin splitting is maximized for the so called *bridge* stacking configuration in which the carbon-carbon links of the GNR cross the boron-nitride links of hBN and for configurations close to the AA stacking configuration, but not for the AA stacking configuration itself. For a zigzag GNR of width $N = 4$ we find that the spin splitting of the conduction and valence bands can be maximized, by varying the stacking configuration, to about 40 meV conservatively assuming a GNR-hBN distance equal to 3.5Å.

Our results show that hBN in general modifies the low energy features of GNRs and that this effect can be tuned to some extent by varying the stacking configuration. For zigzag GNRs, due the spin-sublattice locking of the edges states, the presence of hBN induces a spin splitting of the conduction and valence bands that can be exploited, by properly doping the GNRs, to drive the ribbon into a half-metallic state. The ability to achieve a relatively large spin splitting of the conduction and valence bands without introducing external magnetic fields or proximity to ferromagnetic materials could be very helpful in spintronics applications and in particular to realize quasi 1D ideal spin-filters. In addition, by proximitizing the ribbon to a superconducting system with spin-orbit coupling, such as the surface of Pb, it should be possible to drive a ZGNR-hBN heterostructure in a quasi one-dimensional topological superconducting state.

V. ACKNOWLEDGMENTS

We thank Eric Walters for discussions. This work was supported by NSF Grant No. DMR-1455233, and ONR-N00014-16-1-3158. The numerical calculations have been performed on computing facilities at William & Mary which were provided by contributions from the National Science Foundation, the Commonwealth of Virginia Equipment Trust Fund, and ONR.

[1] K. Nakada, M. Fujita, G. Dresselhaus, and M. S. Dresselhaus, Phys. Rev. B **54**, 17954 (1996).
[2] M. Ezawa, Phys. Rev. B **73**, 045432 (2006).
[3] V. Barone, O. Hod, and G. E. Scuseria, Nano Letters **6**, 2748 (2006), pMID: 17163699.
[4] M. Fujita, K. Wakabayashi, K. Nakada, and K. Kusakabe, Journal of the Physical Society of Japan **65**, 1920 (1996).
[5] Y.-W. Son, M. L. Cohen, and S. G. Louie, Phys. Rev. Lett. **97**, 216803 (2006).
[6] L. Yang, C.-H. Park, Y.-W. Son, M. L. Cohen, and S. G. Louie, Phys. Rev. Lett. **99**, 186801 (2007).
[7] S. Dutta and S. K. Pati, Journal of Materials Chemistry **20**, 8207 (2010).
[8] J. J. Palacios, J. Fernandez-Rossier, L. Brey, and H. A. Fertig, Semiconductor Science Technology **25**, 033003 (2010).
[9] J. Cai, P. Ruffieux, R. Jaafar, M. Bieri, T. Braun, S. Blankenburg, M. Muoth, A. P. Seitsonen, M. Saleh, and X. e. a. Feng, Nature **466**, 470 (2010).
[10] P. Ruffieux, S. Wang, B. Yang, C. Snchez-Snchez, J. Liu, T. Dienel, L. Talirz, P. Shinde, C. A. Pignedoli, and D. e. a. Passerone, Nature **531**, 489 (2016).
[11] A. Narita, X. Feng, Y. Hernandez, S. A. Jensen, M. Bonn, H. Yang, I. A. Verzhbitskiy, C. Casiraghi, M. R. Hansen, and A. H. R. e. a. Koch, Nature Chemistry **6**, 126 (2013).
[12] M. Slota, A. Keerthi, W. K. Myers, E. Tretyakov, M. Baumgarten, A. Ardavan, H. Sadeghi, C. J. Lambert, A. Narita, K. Müllen, and L. Bogani, Nature **557**, 691 (2018).
[13] O. Gröning, S. Wang, X. Yao, C. A. Pignedoli, G. Borin Barin, C. Daniels, A. Cupo, V. Meunier, X. Feng, and A. e. a. Narita, Nature **560**, 209 (2018).
[14] D. J. Rizzo, G. Veber, T. Cao, C. Bronner, T. Chen, F. Zhao, H. Rodriguez, S. G. Louie, M. F. Crommie, and F. R. Fischer, Nature **560**, 204 (2018).
[15] R. M. Lutchyn, E. P. A. M. Bakkers, L. P. Kouwenhoven, P. Krogstrup, C. M. Marcus, and Y. Oreg, Nature Reviews Materials **3**, 52 (2018).
[16] A. C. Potter and P. A. Lee, Phys Rev B **83**, 184520 (2011).
[17] A. C. Potter and P. A. Lee, Phys Rev B **84**, 059906 (2011).
[18] A. M. Lobos, R. M. Lutchyn, and S. Das Sarma, Phys Rev Lett **109**, 146403 (2012).
[19] R. M. Lutchyn, T. D. Stanescu, and S. Das Sarma, Phys Rev B **85**, 140513 (2012).
[20] J. D. Sau and S. Das Sarma, Phys Rev B **88**, 064506 (2013).
[21] H.-Y. Hui, J. D. Sau, and S. Das Sarma, Phys Rev B **92**, 174512 (2015).
[22] J. Zhang, Y. Kim, E. Rossi, and R. M. Lutchyn, Physical Review B **93**, 024507 (2016).
[23] W. S. Cole, J. D. Sau, and S. Das Sarma, Phys Rev B **94**, 140505 (2016).
[24] D. E. Liu, E. Rossi, and R. M. Lutchyn, Phys. Rev. B **97**, 161408 (2018).
[25] A. E. Antipov, A. Bargerbos, G. W. Winkler, B. Bauer, E. Rossi, and R. M. Lutchyn, Phys. Rev. X **8**, 031041 (2018).
[26] B. D. Woods, T. D. Stanescu, and S. Das Sarma, Phys. Rev. B **98**, 035428 (2018).
[27] A. E. G. Mikkelsen, P. Kotetes, P. Krogstrup, and K. Flensberg, Phys. Rev. X **8**, 031040 (2018).
[28] J. Klinovaja and D. Loss, Physical Review X **3**, 011008 (2013), 1211.2739 .
[29] C. R. Dean, A. F. Young, I. Meric, C. Lee., L. Wang, S. Sorgenfrei, K. Watanabe, T. Taniguchi, P. Kim, K. L. Shepard, and J. Hone, Nature Nanotechnology **5**, 726 (2010).
[30] W. Yang, G. Chen, Z. Shi, C.-C. Liu, L. Zhang, G. Xie, M. Cheng, D. Wang, R. Yang, and D. e. a. Shi, Nature Materials **12**, 792 (2013).
[31] J. Xue, J. Sanchez-Yamagishi, D. Bulmash, P. Jacquod, A. Deshpande, K. Watanabe, T. Taniguchi, P. Jarillo-Herrero, and B. J. Leroy, Nat. Mat. **10**, 282 (2011).
[32] L. A. Ponomarenko, A. K. Geim, A. A. Zhukov, R. Jalil, S. V. Morozov, K. S. Novoselov, I. V. Grigorieva, E. H. Hill, V. V. Cheianov, V. I. Fal'Ko, K. Watanabe, T. Taniguchi, and R. V. Gorbachev, Nature Physics **7**, 958 (2011).
[33] M. Yankowitz, J. Xue, D. Cormode, J. D. Sanchez-Yamagishi, K. Watanabe, T. Taniguchi, P. Jarillo-Herrero, P. Jacquod, and B. J. Leroy, Nature Physics **8**, 382 (2012).
[34] K. S. Novoselov, A. K. Geim, S. V. Morozov, D. Jiang, Y. Zhang, S. V. Dubonos, I. V. Grigorieva, and A. A. Firsov, Science **306**, 666 (2004).
[35] K. Nomura and A. H. MacDonald, Phys. Rev. Lett. **96**, 256602 (2006).
[36] Y.-W. Tan, Y. Zhang, K. Bolotin, Y. Zhao, S. Adam, E. H. Hwang, S. Das Sarma, H. L. Stormer, and P. Kim, Phys. Rev. Lett. **99**, 246803 (2007).
[37] E. H. Hwang, S. Adam, and S. D. Sarma, Phys. Rev. Lett. **98**, 186806 (2007).
[38] S. D. Sarma, E. H. Hwang, and E. Rossi, Phys. Rev. B **81**, 161407(R) (2010).
[39] S. Das Sarma, S. Adam, E. H. Hwang, and E. Rossi, Rev. Mod. Phys. **83**, 407 (2011).
[40] S. Adam, E. H. Hwang, V. M. Galitski, and S. Das Sarma, Proceedings of the National Academy of Sciences **104**, 18392 (2007).
[41] M. M. Fogler, D. S. Novikov, and B. I. Shklovskii, Phys. Rev. B **76**, 233402 (2007).
[42] E. Rossi and S. Das Sarma, Phys. Rev. Lett. **101**, 166803 (2008).
[43] M. Polini, A. Tomadin, R. Asgari, and A. H. MacDonald, Phys. Rev. B **78**, 115426 (2008).
[44] S. Adam, S. Cho, M. S. Fuhrer, and S. Das Sarma, Phys. Rev. Lett. **101**, 046404 (2008).
[45] M. M. Fogler, Phys. Rev. Lett. **103**, 236801 (2009).
[46] E. Rossi, S. Adam, and S. D. Sarma, Phys. Rev. B **79**, 245423 (2009).
[47] E. Rossi and S. Das Sarma, Phys. Rev. Lett. **107**, 155502 (2011).
[48] Q. Li, E. H. Hwang, E. Rossi, and S. Das Sarma, Phys. Rev. Lett. **107**, 156601 (2011).
[49] D. S. L. Abergel, E. Rossi, and S. Das Sarma, Phys. Rev. B **86**, 155447 (2012).
[50] D. S. L. Abergel, M. Rodriguez-Vega, E. Rossi, and S. Das Sarma, Phys. Rev. B **88**, 235402 (2013).

[51] Q. Li, E. Hwang, and E. Rossi, Solid State Communications **152**, 1390 (2012), exploring Graphene, Recent Research Advances.
[52] J. Zhang and E. Rossi, Phys. Rev. Lett. **111**, 086804 (2013).
[53] J. Zhang, C. Triola, and E. Rossi, Phys. Rev. Lett. **112**, 096802 (2014).
[54] M. Rodriguez-Vega, J. Fischer, S. Das Sarma, and E. Rossi, Phys. Rev. B **90**, 035406 (2014).
[55] M. Rodriguez-Vega, G. Schwiete, J. Sinova, and E. Rossi, Phys. Rev. B **96**, 235419 (2017).
[56] C.-P. Lu, M. Rodriguez-Vega, G. Li, A. Luican-Mayer, K. Watanabe, T. Taniguchi, E. Rossi, and E. Y. Andrei, Proceedings of the National Academy of Sciences **113**, 6623 (2016).
[57] J. C. W. Song, A. V. Shytov, and L. S. Levitov, Phys. Rev. Lett. **111**, 266801 (2013).
[58] J. Jung, A. Raoux, Z. Qiao, and A. H. MacDonald, Phys. Rev. B **89**, 205414 (2014).
[59] J. C. W. Song, P. Samutpraphoot, and L. S. Levitov, Proc. National Acad. Sciences United States Am. **112**, 10879 (2015).
[60] J. Jung, A. M. DaSilva, A. H. MacDonald, and S. Adam, Nature Communicationsxxxx **6**, 6308 (2015).
[61] J. Jung, E. Laksono, A. M. DaSilva, A. H. MacDonald, M. Mucha-Kruczyński, and S. Adam, Phys. Rev. B **96**, 085442 (2017).
[62] L. Britnell, R. V. Gorbachev, R. Jalil, B. D. Belle, F. Schedin, A. Mishchenko, T. Georgiou, M. I. Katsnelson, L. Eaves, and S. V. e. a. Morozov, Science **335**, 947 (2012).
[63] B. Hunt, J. D. Sanchez-Yamagishi, A. F. Young, M. Yankowitz, B. J. LeRoy, K. Watanabe, T. Taniguchi, P. Moon, M. Koshino, and P. e. a. Jarillo-Herrero, Science **340**, 1427 (2013).
[64] L. A. Ponomarenko, R. V. Gorbachev, G. L. Yu, D. C. Elias, R. Jalil, A. A. Patel, A. Mishchenko, A. S. Mayorov, C. R. Woods, and J. R. e. a. Wallbank, Nature **497**, 594 (2013).
[65] C. R. Dean, L. Wang, P. Maher, C. Forsythe, F. Ghahari, Y. Gao, J. Katoch, M. Ishigami, P. Moon, and M. e. a. Koshino, Nature **497**, 598 (2013).
[66] C. R. Woods, L. Britnell, A. Eckmann, R. S. Ma, J. C. Lu, H. M. Guo, X. Lin, G. L. Yu, Y. Cao, and R. V. e. a. Gorbachev, Nature Physics **10**, 451 (2014).
[67] Y. Zhang, Y.-W. Tan, H. L. Stormer, and P. Kim, Nature **438**, 201 (2005).
[68] A. H. Castro Neto, F. Guinea, N. M. R. Peres, K. S. Novoselov, and A. K. Geim, Rev. Mod. Phys. **81**, 109 (2009).
[69] L. C. Campos, V. R. Manfrinato, J. D. Sanchez-Yamagishi, J. Kong, and P. Jarillo-Herrero, Nano Letters **9**, 2600 (2009).
[70] D. Gunlycke and C. T. White, Phys. Rev. B **77**, 115116 (2008).
[71] H. Zheng, Z. F. Wang, T. Luo, Q. W. Shi, and J. Chen, Phys. Rev. B **75**, 165414 (2007).
[72] L. Brey and H. A. Fertig, Phys. Rev. B **73**, 235411 (2006).
[73] H. Raza and E. C. Kan, Physical Review B **77**, 245434 (2008).
[74] B. Sahu, H. Min, A. H. MacDonald, and S. K. Banerjee, Physical Review B **78**, 045404 (2008).
[75] G. Lee and K. Cho, Phys. Rev. B **79**, 165440 (2009).
[76] H. Lee, Y.-W. Son, N. Park, S. Han, and J. Yu, Phys. Rev. B **72**, 174431 (2005).
[77] Y.-W. Son, M. L. Cohen, and S. G. Louie, Phys. Rev. Lett. **97**, 216803 (2006).
[78] M. Kan, J. Zhou, Q. Sun, Q. Wang, Y. Kawazoe, and P. Jena, Phys. Rev. B **85**, 155450 (2012).
[79] P. Giannozzi, S. Baroni, N. Bonini, M. Calandra, R. Car, C. Cavazzoni, D. Ceresoli, G. L. Chiarotti, M. Cococcioni, I. Dabo, A. D. Corso, S. de Gironcoli, S. Fabris, G. Fratesi, R. Gebauer, U. Gerstmann, C. Gougoussis, A. Kokalj, M. Lazzeri, L. Martin-Samos, N. Marzari, F. Mauri, R. Mazzarello, S. Paolini, A. Pasquarello, L. Paulatto, C. Sbraccia, S. Scandolo, G. Sclauzero, A. P. Seitsonen, A. Smogunov, P. Umari, and R. M. Wentzcovitch, Journal of Physics: Condensed Matter **21**, 395502 (2009).
[80] J. P. Perdew, K. Burke, and M. Ernzerhof, Phys. Rev. Lett. **77**, 3865 (1996).
[81] D. Soriano and J. Fernández-Rossier, Phys. Rev. B **85**, 195433 (2012).
[82] Y.-W. Son, M. L. Cohen, and S. G. Louie, Nature **444**, 347 (2006).
[83] J. Yu and W. Guo, The Journal of Physical Chemistry Letters **4**, 951 (2013).